Active control of turbulent boundary layer sound transmission into a vehicle interior

A Caiazzo, N Alujević, B Pluymers and W Desmet

KU Leuven, Department of Mechanical Engineering, Celestijnenlaan 300B, 3001 Heverlee, Belgium.

E-mail: Anna.Caiazzo@kuleuven.be

Abstract. In high speed automotive, aerospace, and railway transportation, the turbulent boundary layer (TBL) is one of the most important sources of interior noise. The stochastic pressure distribution associated with the turbulence is able to excite significantly structural vibration of vehicle exterior panels. They radiate sound into the vehicle through the interior panels. Therefore, the air flow noise becomes very influential when it comes to the noise vibration and harshness assessment of a vehicle, in particular at low frequencies. Normally, passive solutions, such as sound absorbing materials, are used for reducing the TBL-induced noise transmission into a vehicle interior, which generally improve the structure sound isolation performance. These can achieve excellent isolation performance at higher frequencies, but are unable to deal with the low-frequency interior noise components. In this paper, active control of TBL noise transmission through an acoustically coupled double panel system into a rectangular cavity is examined theoretically. The Corcos model of the TBL pressure distribution is used to model the disturbance. The disturbance is rejected by an active vibration isolation unit reacting between the exterior and the interior panels. Significant reductions of the low-frequency vibrations of the interior panel and the sound pressure in the cavity are observed.

1. Introduction

The interior noise in high speed vehicles is largely caused by the aerodynamic excitation of the vehicle exterior skin panels. For example, the predominant contributor to the interior noise in passenger aircraft at the cruise speed is the TBL [1, 2, 3]. The character of the TBL excitation is such that it is random and broadband. Thus the disturbance comes in a wide range of frequencies including the low-frequency range. Normally, the effectiveness of passive noise control methods, such as sound absorbing materials, is limited to frequencies where the acoustic wavelengths are short and thus the frequency is relatively large. As a rule of thumb, the thickness of sound absorbing layers should be at least 1/4 of the acoustic wavelength. As a result, the passive sound absorbing treatments consume too much space and weight if the sound transmission control is to be extended to low frequencies. On the other hand, double leaf partitions may be used whose transmission loss increases more rapidly with frequency than that of single leaf partitions. Therefore, it is often the case that vehicles are equipped with additional interior trim panels. Nevertheless, at frequencies below the mass-air-mass resonance, the transmission loss of double leaf partitions is still rather poor. For these reasons, an interest has grown in investigating into active methods for the control of low-frequency sound transmission through double panels. Active control of sound transmission can be used both with deterministic and

stochastic disturbances. Feedforward and feedback active control systems have been considered in this sense. Although feedforward control methods are more easily applied for the control of deterministic, tonal disturbances, it is also possible to use them to control stochastic noise. This, however, requires that creative arrangements are used for obtaining reference signals well correlated to the disturbance [4, 5]. Here a good balance between the causality margin and the coherence between the reference and disturbance signals is essential [5]. Feedback sound transmission control systems can be used instead, and some promising results have been reported in the last decade [3, 6, 7]. In the feedback control it is often useful to collocate dual sensor-actuator pairs in order to minimise or avoid the modelling effort. However, fully dual and collocated sensor-actuator pairs are not straightforward to realise in practice. Nevertheless, some very convincing collocated feedback control methods have been proposed for vibration isolation in lumped parameter systems [8, 9, 10]. In this paper the active vibration isolation method, sometimes referred to as "skyhook damping" [8], is applied to control the sound transmission through a double panel system into a model vehicle interior. It is shown in the paper that very good low-frequency active sound transmission control can be realised using this approach, even though only a single feedback loop has been considered. The paper is structured as follows. In the second section, a brief outline of the mathematical model used to couple the aerodynamic, control and vibroacoustic aspects of the problem is given. In the third section, the stability and performance of the active control system is discussed on a reduced order model, whereas in the fourth section a full-order model is considered.

2. Model Problem

The analytical model outlined in this section is used to predict the noise transmission through an acoustically coupled double panel system into a rectangular cavity when an active vibration isolation unit is used. The problem under analysis is physically given by the interaction of an aerodynamic model, that represents the TBL pressure fluctuations on the structure, and a structural-acoustic model, that gives the noise transmission and interior noise levels. The model is thus similar to the problem of sound transmission into a vehicle interior.

2.1. Aerodynamic model

In a wide variety of experimental situations, it has been found that the flow near boundaries can be modelled as stochastic fluctuations riding on a steady current. Therefore, mathematical models of TBL wall pressure take the form of a statistical space-time correlation function, and its corresponding Fourier transform or wavevector-frequency spectrum. Among the different TBL models developed over the years [11], the Corcos' one is the simplest empirical model used to represent the wall pressure fluctuation of a TBL [12, 13]. In general, the wall pressure field, generated by a fully developed TBL with zero mean pressure gradient, can be regarded as homogeneous in space and stationary in time. For a flow in the x-direction over the (x, y) plane, the spatial-cross spectral density CSD, according to Corcos, is given by

$$\Psi_{pp}(\zeta_x, \zeta_y, \omega) = \phi(\omega) \mathrm{e}^{-\mathrm{i}k_\omega \zeta_x} \mathrm{e}^{-|\zeta_x| k_\omega \alpha_x - |\zeta_y| k_\omega \alpha_y}, \tag{1}$$

where $k_\omega = \omega/U_c$ is the convective wavenumber, given by the angular frequency ω and the convective velocity $U_c = 0.6U_\infty$, and $\zeta \equiv (\zeta_x, \zeta_y, 0)$ is the spatial separation vector. The longitudinal and lateral decay rates of the coherences, α_x and α_y respectively, are normally chosen to yield good agreement with experiments [14]. In the following analysis, the external flow properties used, including α_x and α_y, are identical to those defined by Rocha [15], in which $U_\infty = 0.8c$ with c speed of sound. In Eq. (1), $\phi(\omega)$ represents the single point wall-pressure spectrum (*i.e.*, auto-spectrum). It is given by a semi-empirical formula published by Goody [16]

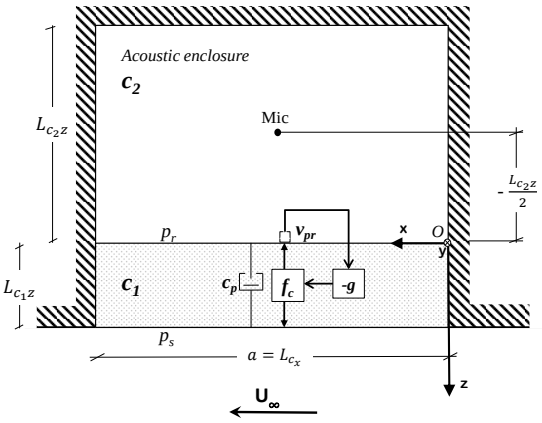

Figure 1. The model problem.

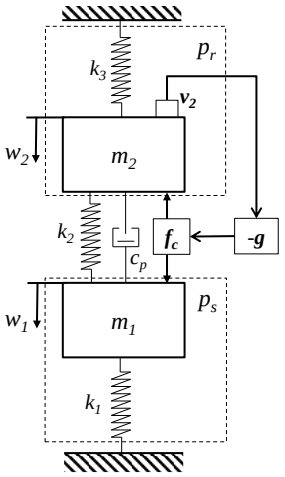

Figure 2. Reduced order model.

as follows,

$$\phi(\omega) = \frac{3\left(\delta/U_\infty\right)^3\left(\omega\tau_\omega\right)^2}{\left[\left(\omega\delta/U_\infty\right)^{0.75}+0.5\right]^{3.7}+\left[\left(1.1R_T^{-0.57}\right)\left(\omega\delta/U_\infty\right)\right]^7}, \tag{2}$$

in which δ is the boundary layer thickness, R_T is the Reynolds number dependent factor and τ_ω is the wall shear stress. Such a model compares well with experimental data over a large range of Reynolds numbers [17].

2.2. Structural-acoustic model

In Fig. 1, the analysed model problem is shown. The model encompasses a cavity-backed homogeneous double panel driven on one side by a stationary TBL, described in Eq. (1). Thus, the acoustic enclosure, c_2, filled with air, has five rigid walls and one flexible double wall. The two flexible panels are acoustically coupled with the air in cavity c_1 between them. As shown in Fig. 1, the source panel is excited by the grazing flow. Its vibrations generate sound waves which excite the radiating panel. Finally, the vibrations of the radiating panel generate sound waves which are radiated to the acoustic enclosure c_2. The active control approach in this study is based on isolating the radiating panel from vibrations coming from the source panel through an active vibration isolation unit. A sensor is placed in the centre of the radiating panel, which is collocated to a reactive force actuator. The actuator generates the control force while reacting against the source panel. In parallel to the actuator, a passive damper is mounted with a damping coefficient c_p, as seen in Fig. 1. In this paper, idealized sensor-actuator transducers are considered, that is, the sensor-actuator internal dynamics are not taken into account. The control force f_c is made proportional to the negative velocity of the radiating panel, v_{p_r}, which is measured by the velocity sensor, so that

$$f_c = -g v_{p_r}, \tag{3}$$

where g is the feedback gain. Its dimension is the same as that of the damping coefficient, Nsm^{-1}. Therefore, there are two damping coefficients, the active damping coefficient g and the passive one c_p. In order to model the structural-acoustic control problem at hand, the panel displacements and acoustic enclosure pressures are calculated by coupling the wave equations for the two cavities with the governing equations for the two panels [15, 18]. To this end, the modal expansion method is used [15, 18]. Simply supported boundaries of the two panels, and

rigid cavity walls are assumed. The rectangular coordinates (x, y, z) are chosen, z being normal to the panel, and x in the direction of mean flow, as seen in Fig. 1. The pressure field on the flow side of the plate consists of the sum of the turbulence pressure, $p_{tbl}(x, y, z, t)$, which would be observed on a rigid wall and the pressure due to the contribution of the acoustic enclosure c_1. The influence of the panel vibration on the boundary layer is neglected, that is, a weak coupling is considered [19]. The system is analysed by expanding the displacements of the source and radiating panels and the pressure of the acoustic cavities in a series of characteristic functions, that are in-vacuo modes of a simply supported plate and acoustic modes of a rigid rectangular enclosure,

$$w_i(x, y, t) = \sum_{m_x, m_y}^{M_{x_i}, M_{y_i}} d_{i_{m_x m_y}}(t)\psi_{i_{m_x m_y}}(x, y), \tag{4}$$

with $i = p_s, p_r$ for the source and radiating panel respectively, and

$$p_c(x, y, z, t) = \sum_{n_x, n_y, n_z}^{N_{xc}, N_{yc}, N_{zc}} g_{c_{n_x n_y n_z}}(t)\Gamma_{c_{n_x n_y n_z}}(x, y, z), \tag{5}$$

with $c = c_1, c_2$ for the cavity of the double panel system and the back cavity respectively, as shown in Fig. 1. The modal functions are defined as follows,

$$\psi_{i_{m_x m_y}}(x, y) = \frac{2}{\sqrt{a_i b_i}} \sin(m_x \pi x/a_i) \sin(m_y \pi y/b_i), \tag{6}$$

$$\Gamma_{c_{n_x n_y n_z}}(x, y, z) = \frac{A_{n_x} A_{n_y} A_{n_z}}{\sqrt{L_{c_x} L_{c_y} L_{c_z}}} \cos(n_x \pi x/L_{c_x}) \cos(n_y \pi y/L_{c_y}) \cos(n_z \pi z/L_{c_z}), \tag{7}$$

in which $d_{i_{m_x m_y}}(t)$ and $g_{c_{n_x n_y n_z}}(t)$ are components of the displacements and pressure time functions, respectively. The total number of plate modes is $\mathrm{M}_i = \mathrm{M}_{x_i} \times \mathrm{M}_{y_i}$ and for the acoustics modes is $\mathrm{N}_c = \mathrm{N}_{x_c} \times \mathrm{N}_{y_c} \times \mathrm{N}_{z_c}$. The plates have length a and width b; L_{c_x}, L_{c_y} and L_{c_z} are acoustic enclosure length, width and height, respectively. In Eq. (7), A_n equals to $\sqrt{2}$ when $n \neq 0$ and equal to 1 when $n = 0$. The matrix form of the coupled structural acoustic system can be expressed, in the frequency domain, as [18]:

$$\mathbf{Y}(\omega) = \mathbf{H}(\omega)\,\mathbf{X}(\omega), \tag{8}$$

where

$$\mathbf{Y}(\omega) = \begin{Bmatrix} \mathbf{D}_{p_s}(\omega) \\ \mathbf{G}_{c_1}(\omega) \\ \mathbf{D}_{p_r}(\omega) \\ \mathbf{G}_{c_2}(\omega) \end{Bmatrix}, \qquad \mathbf{X}(\omega) = \begin{Bmatrix} \mathbf{P}_{tbl}(\omega) \\ \mathbf{0} \\ \mathbf{0} \\ \mathbf{0} \end{Bmatrix},$$

in which $\mathbf{D}_i(\omega)$, $\mathbf{G}_c(\omega)$ and $\mathbf{P}_{tbl}(\omega)$ are the frequency domain vectors of the displacements, pressure and turbulence pressure, respectively. The frequency response matrix of the system is given by $\mathbf{H}(\omega)$,

$$\mathbf{H}(\omega) = \begin{bmatrix} \mathbf{H}_{11}(\omega) & \mathbf{K}_{p_s c_1} & \mathrm{i}\omega\mathbf{D}_{p_s p_r} & \mathbf{0} \\ -\omega^2\mathbf{M}_{c_1 p_s} & \mathbf{H}_{22}(\omega) & -\omega^2\mathbf{M}_{c_1 p_r} & \mathbf{0} \\ \mathrm{i}\omega\mathbf{D}_{p_r p_s} & \mathbf{K}_{p_r c_1} & \mathbf{H}_{33}(\omega) & \mathbf{K}_{p_r c_2} \\ \mathbf{0} & \mathbf{0} & -\omega^2\mathbf{M}_{c_2 p_r} & \mathbf{H}_{44}(\omega) \end{bmatrix}^{-1},$$

with

$$\mathbf{H}_{11}(\omega) = -\omega^2\mathbf{M}_{p_s p_s} + \mathrm{i}\omega\mathbf{D}_{p_s p_s} + \mathbf{K}_{p_s p_s}, \qquad \mathbf{H}_{22}(\omega) = -\omega^2\mathbf{M}_{c_1 c_1} + \mathrm{i}\omega\mathbf{D}_{c_1 c_1} + \mathbf{K}_{c_1 c_1}, \tag{9}$$

$$\mathbf{H}_{33}(\omega) = -\omega^2\mathbf{M}_{p_rp_r} + \mathrm{i}\omega\mathbf{D}_{p_rp_r} + \mathbf{K}_{p_rp_r}, \qquad \mathbf{H}_{44}(\omega) = -\omega^2\mathbf{M}_{c_2c_2} + \mathrm{i}\omega\mathbf{D}_{c_2c_2} + \mathbf{K}_{c_2c_2}. \quad (10)$$

The contributions of the passive damping force and the active damping force are contained in $\mathbf{H}(\omega)$ as follows,

$$\mathbf{D}_{p_sp_s} = \mathrm{diag}\left[2\rho t\omega_m\sigma\right]_{p_s} + c_p\boldsymbol{\psi}^2_{p_{s_{m_xm_y}}}, \qquad \mathbf{D}_{p_rp_s} = -c_p\boldsymbol{\psi}_{p_{s_{m_xm_y}}}\boldsymbol{\psi}_{p_{r_{m_xm_y}}}, \quad (11)$$

$$\mathbf{D}_{p_sp_r} = -(g+c_p)\,\boldsymbol{\psi}_{p_{s_{m_xm_y}}}\boldsymbol{\psi}_{p_{r_{m_xm_y}}}, \qquad \mathbf{D}_{p_rp_r} = \mathrm{diag}\left[2\rho t\omega_m\sigma\right]_{p_r} + (g+c_p)\,\boldsymbol{\psi}^2_{p_{r_{m_xm_y}}}, \quad (12)$$

where ρ, t and σ are the density, thickness and structural damping ratio of the panels and ω_m are the natural frequencies of the panels. Since the TBL excitation is defined in terms of power spectral density of the wall pressure, it is convenient to write the coupled system governing equations in the power spectral density (PSD) domain,

$$\mathbf{S}_{\mathbf{YY}}(\omega) = \mathbf{H}^*(\omega)\,\mathbf{S}_{\mathbf{XX}}(\omega)\,\mathbf{H}^{\mathbf{T}}(\omega), \quad (13)$$

where $\mathbf{S}_{\mathbf{XX}}(\omega)$ is the PSD matrix of the random excitation, which includes the PSD matrix of the TBL pressure; $\mathbf{S}_{\mathbf{YY}}(\omega)$ is the PSD matrix of the plate displacements, $\mathbf{S}_{\mathbf{WW}_i}(\omega)$, and the acoustic pressures, $\mathbf{S}_{\mathbf{PP}_c}(\omega)$, and the superscripts $*$ and T denote Hermitian and matrix transpose, respectively. The PSD matrix of the TBL pressure is given by,

$$\mathbf{S}_{tbl}(\omega) = \left[\iint_0^{a_{p_s}}\iint_0^{b_{p_s}} \psi_{p_{s_{m_xm_y}}}(x,y)\psi_{p_{s_{m_{x'}m_{y'}}}}(x',y')\,\Psi_{pp}(\zeta_x,\zeta_y,\omega)\,\mathrm{dx}\mathrm{dx}'\,\mathrm{dy}\mathrm{dy}'\right]. \quad (14)$$

After some mathematical manipulations, the PSD functions of the plate displacement (and velocity) and the acoustic enclosure pressure in a specific point inside the enclosure can be defined,

$$\mathbf{S}_{ww_i}(x_1,y_1,x_2,y_2,\omega) = \sum_{m_{x_1},m_{x_2}}^{M_{x_i}^2}\sum_{m_{y_1},m_{y_2}}^{M_{y_i}^2} \psi_{i_{m_{x_1}m_{y_1}}}(x_1,y_1)\psi_{i_{m_{x_2}m_{y_2}}}(x_2,y_2)S_{WWi_{m_1,m_2}}(\omega), \quad (15)$$

$$\begin{aligned}\mathbf{S}_{pp_c}(x_1,y_1,z_1,x_2,y_2,z_2,\omega) = \sum_{n_{x_1},n_{x_2}}^{N_{x_c}^2}\sum_{n_{y_1},n_{y_2}}^{N_{y_c}^2}\sum_{n_{z_1},n_{z_2}}^{N_{z_c}^2} &\Gamma_{c_{n_{x_1}n_{y_1}n_{z_1}}}(x_1,y_1,z_1)\\ &\times\Gamma_{c_{n_{x_2}n_{y_2}n_{z_2}}}(x_2,y_2,z_2)S_{PPc_{n_1,n_2}}(\omega).\end{aligned} \quad (16)$$

Afterwards, the radiating body velocity PSD is given by

$$\mathbf{S}_{vv_i}(x_1,y_1,x_2,y_2,\omega) = \omega^2\mathbf{S}_{ww_i}(x_1,y_1,x_2,y_2,\omega). \quad (17)$$

3. Results with a reduced order model

In this section, the theoretical stability and performance analysis of the active control system are carried out by using a simplified model. The simplified model is obtained by considering only the first mode for each plate and each air cavity. Note that the first mode of each air cavity corresponds to a zero resonance frequency. The resulting system then behaves exactly as a two degree of freedom (DOF) model, which can be represented through equivalent coefficients m_1, m_2, k_1, k_2, k_3, as shown in Fig. 2. The equivalent coefficients can be directly calculated using Eq. (8), but their derivation in this paper is omitted for brevity. Given that only zero frequency mode is assumed for the two cavities, the pressures inside the cavities are uniform. Thus, the stiffness of the air enclosed in c_1 can be represented by stiffness k_2, and the stiffness of the air enclosed in c_2 contributes to the stiffness k_3. In the following section, the stability of the feedback loop, shown in Fig. 2, is analysed using the Routh-Hurwitz criterion.

3.1. Stability

The characteristic equation of the reduced order model shown in Fig. 2 is of the form:

$$A_4 s^4 + A_3 s^3 + A_2 s^2 + A_1 s + A_0 = 0, \tag{18}$$

with $s = \mathrm{i}\omega$. The coefficients A_i, seen in Eq. 18, can be found, for example, in [9, 10]. The system is stable if all roots of the characteristic equation have negative real parts. The Routh-Hurwitz criterion can be used to verify this. According to this criterion, the necessary condition for the stability is that all coefficients of the characteristic equation are positive. Additionally, all the principal diagonal minors Δ_i of the Hurwitz matrix must be positive. This results in a system of inequalities, which can be solved for the active damping ratio $\xi = g/c_p$ by introducing the following non-dimensional parameters:

$$\mu = \frac{m_2}{m_1}, \qquad \alpha = \left(\frac{\Omega_2}{\Omega_1}\right)^2, \qquad \beta = \left(\frac{\Omega_3}{\Omega_1}\right)^2, \qquad \eta = \frac{c_p}{2\sqrt{k_1 m_1}}, \tag{19}$$

where $\Omega_1 = \sqrt{k_1/m_1}$, $\Omega_2 = \sqrt{k_2/m_2}$ and $\Omega_3 = \sqrt{k_3/m_2}$, μ is the mass ratio, α and β are the frequency ratios and η is the passive damping ratio. Here, the stability of the system is found to substantially depend on the frequency ratio β. In case $\beta > 1$, the system is stable if the active damping ratio is between two bordering values given by

$$\xi_{1,2} = -\frac{\alpha\,(1+\mu) + 1 - \beta \mp \sqrt{(1+\mu)^2\,\alpha^2 - 2\alpha\,(\beta-1)\,(\mu-1) + (\beta-1)^2}}{2\alpha}. \tag{20}$$

This is because, as shown in Fig. 3, all principal diagonal minors Δ_i are positive if $\xi_1 > \xi > \xi_2$. On the contrary, if $\beta < 1$ then the system is stable for any $\xi > \xi_1$, as shown in Fig. 4. The property of the systems corresponding to Fig. 3 -4 are shown in Table 1. The variations of the frequency ratio β is accomplished by changing the thicknesses of the two panels. Note that in both cases it is the fourth principal diagonal minor Δ_4, characterised by a quadratic dependence on ξ, that governs the system stability. In conclusion, the range of stable feedback gains is found as follows:

$$\forall \beta > 1, \quad \xi_1 > \xi > \xi_2, \tag{21}$$

$$\forall \beta < 1, \quad \xi > \xi_1. \tag{22}$$

Table 1. Model properties.

Plate length a (m)	0.4	Cavity length L_{c_x} (m)	0.4
Plate width b (m)	0.3	Cavity width L_{c_y} (m)	0.3
Plate Elasticity Modulus E (GPa)	100	Cavity height $L_{c_{1_z}}$ (m)	0.038
Plate density ρ (kg m^{-3})	2380	Cavity height $L_{c_{2_z}}$ (m)	0.4
Plate Poisson's ratio ν	0.33	Acoustic damping ratio σ_{ac}	0.05
Air speed of sound c_0 (m s^{-1})	343	Internal air density ρ_0 (kg m^{-3})	1.19
Plate thickness t_{ps} (m)	0.002 (0.003)	Structural damping ratio σ	0.01
Plate thickness t_{pr} (m)	0.003 (0.002)		

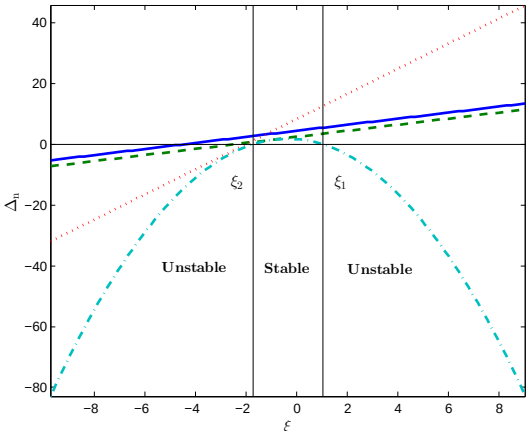

Figure 3. $\beta > 1$: principal diagonal minors,(——) Δ_1, (- - - -) Δ_2, (·····) Δ_3, (— · —) Δ_4.

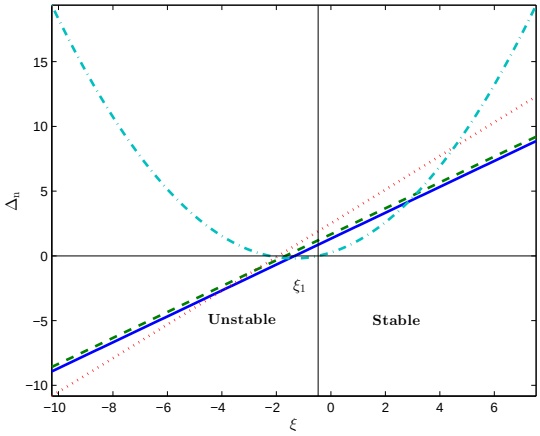

Figure 4. $\beta < 1$: principal diagonal minors,(——) Δ_1, (- - - -) Δ_2, (·····) Δ_3, (— · —) Δ_4.

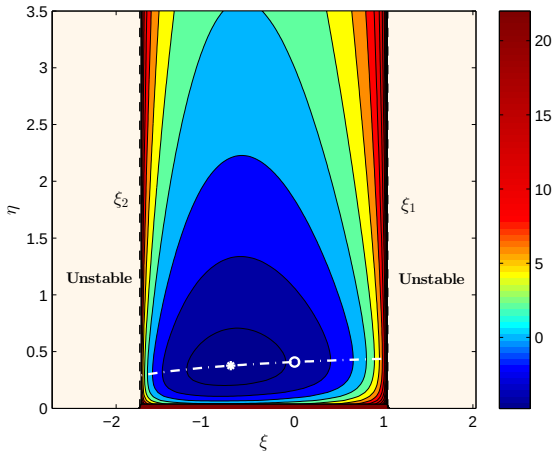

Figure 5. Mean squared velocity of the radiating body plotted versus ξ and η, for $\beta > 1$, in the case of a white noise excitation.

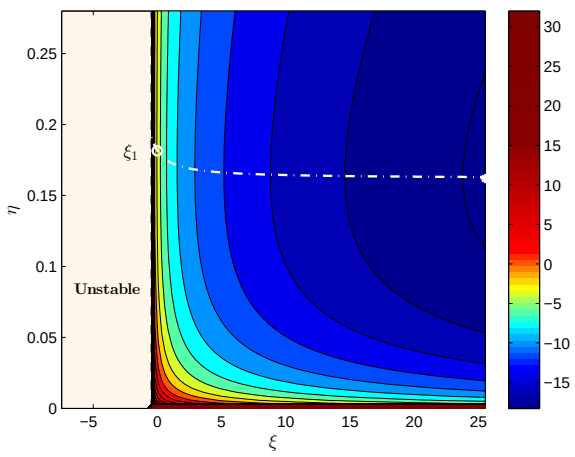

Figure 6. Mean squared velocity of the radiating body plotted versus ξ and η, for $\beta < 1$, in the case of a white noise excitation.

3.2. Performance

The performance of the active control system is analysed in two ways. Firstly, a point force acting on mass m_1 is assumed with a white noise spectral distribution, that corresponds to a force located at the centre of the source panel in Fig. 1. In this case, the mean squared velocity of the radiating body is found by solving the integral over frequencies of the squared magnitude of the system transfer mobility, since a unit power spectral density for the excitation is assumed. Secondly, a TBL excitation on the source panel is assumed. In this case, the frequency- and space-averaged velocity PSD (VPSD) of the radiating plate is used. In either excitation scenario, the performance of the active control is found to be a function of the active and passive damping ratio ξ and η.

3.2.1. Point force excitation In Fig. 5 - 6, the mean squared velocity of the radiating panel is plotted as function of the passive and active damping ratio. The case with $\beta > 1$ is shown

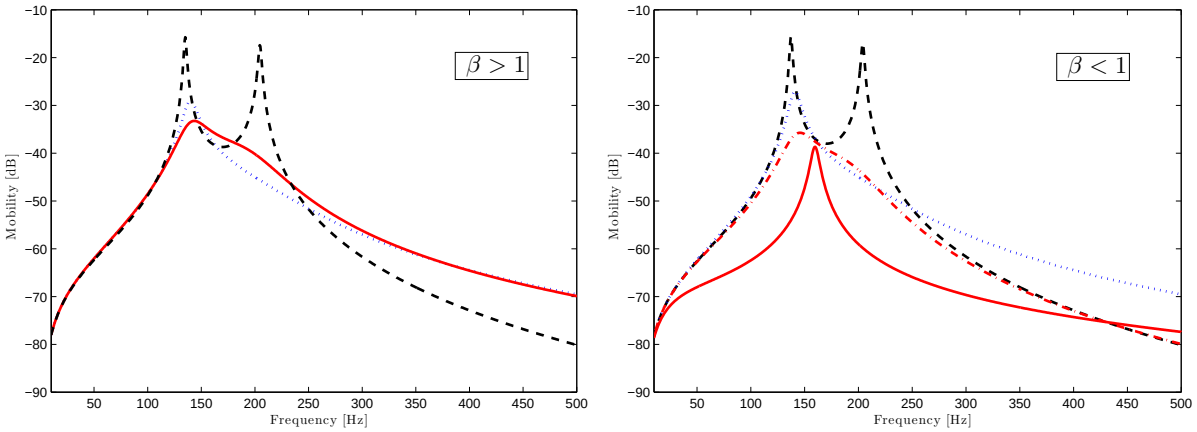

Figure 7. Amplitude of the transfer mobility of the radiating body. No control (- - - -), passive control (·····), optimal tuned active control (——) and for $\beta < 1$, $\eta = \eta_{opt}/10$ (— · —). Left hand side is for $\beta > 1$ and right hand side is for $\beta < 1$.

in Fig. 5, whereas the case with $\beta < 1$ is in Fig. 6. For $\beta > 1$, a minimum exists for a certain combinations of ξ and η and it is indicated in Fig. 5 by a white star "$*$". It corresponds to an optimal combination of the damping coefficients, g_{opt} and $c_{p_{opt}}$. For $\beta < 1$, there is no minimum since the kinetic energy decreases monotonically with ξ and it will continue to decrease with increasing the gain g, so theoretically an infinite reduction of sound power is possible. Therefore, when $\beta < 1$, large absolute values of positive ξ give considerable vibration isolation effects. On the contrary, when $\beta > 1$, the maximum gain is limited between ξ_1 and ξ_2. In both figures, the white dash-dotted line gives an optimal passive damping ratio, η_{opt}, for any stable ξ. In Fig. 7, the amplitude of the transfer mobility of the radiating panel for the two cases is shown. Two control approaches are considered. The first approach is a fully passive approach where the feedback gain equals zero and the damping is achieved exclusively through c_p. The damping coefficient c_p can be tuned to an optimal value which is indicated by a hollow circle in Fig. 5 - 6. The second approach is with a combination of passive and active damping achieved through both the feedback gain and the damper c_p. In this case, the optimally tuned damping ratio, (ξ_{opt}, η_{opt}), defined with the white star "$*$"is used when $\beta > 1$; whereas, for $\beta < 1$, ξ is set to 10. The passive damping ratio is set to a value that lies on the white dash-dotted line in Fig. 6. Comparing the frequency spectra in Fig. 7, it can be seen that the active control (solid line) gives a significant improvement over the passive one. Additionally, it is clear that the situation in which $\beta < 1$ results in a much more convincing active reductions of the radiating panel vibrations in comparison to the situation in which $\beta > 1$.

3.2.2. Turbulent boundary layer excitation In Fig. 8 and 9, the vibration isolation performance of the control system for a stationary TBL excitation, described in Eq. (1), are plotted. Only the case with $\beta < 1$ is considered. Once again, it is possible to define an optimal combination of the active and the passive damping ratios which minimizes the kinetic energy of the radiating panel, as shown by the white dash-dotted line in Fig. 8. As with the point force excitation, the radiating panel kinetic energy decreases monotonically with ξ. However, the stochastic TBL pressure distribution results in a steeper high frequency roll-off of the radiating body velocity PSD (VPSD), shown in Fig. 9. An improvement due to the optimal active control, in comparison with the passive one, is still found (solid line); even when the passive damping ratio is one tenth of the optimal one (dash-dot line). Therefore, also with a TBL excitation, the proposed control

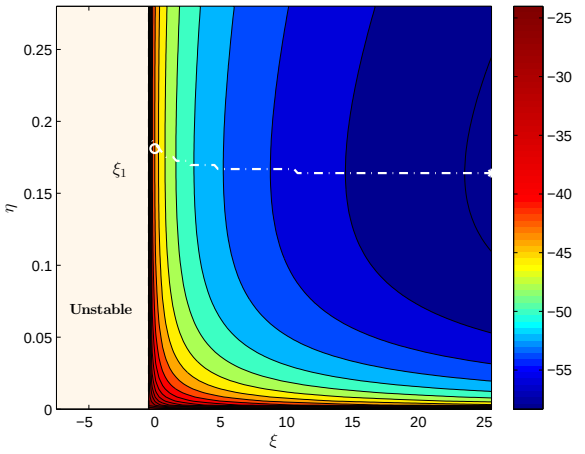

Figure 8. Frequency- and space-averaged VPSD of the radiating body plotted versus ξ and η, for $\beta < 1$, with a TBL excitation

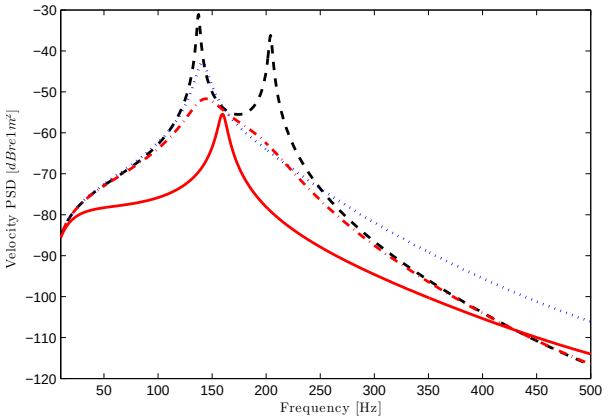

Figure 9. VPSD of the radiating body, for $\beta < 1$, with a TBL excitation. No control (- - - -), passive control (·····) and optimal tuned active control (——), $\eta = \eta_{opt}/10$ (— · —).

approach gives the expected, if not better, results. These results can be generalized also for the sound pressure in the cavity c_2, since for the reduced order model the pressure distributions are uniform due to the zero frequency acoustic breathing mode.

4. Results with an increased order model

In this section, a total number of $M_{p_s} = 24$ and $M_{p_r} = 20$ panel modes, and $N_{c_1} = 24$ and $N_{c_2} = 48$ acoustic modes, is used to model the response of the system up to 1000 Hz. The stability of the control system is again discussed. However, the large number of modes precludes the use of the Routh-Hurwitz criterion such that the Nyquist criterion is used as an alternative. Also, the performance of the active control system is studied in the case with a stationary TBL excitation.

4.1. Stability

The open loop sensor-actuator frequency response function is used to analyse the stability of the feedback loop using the Nyquist criterion. That is, the error velocity measured by the sensor at the radiating panel, p_r, witch is due to the control force, f_c, is considered when the primary excitation is switched off. Note that the error velocity is due to both components of the control force, one acting on radiating panel p_r and the other one reacting off source panel p_s. In Fig. 10 - 11, two Nyquist plots are shown. One for the case with $\beta > 1$ and the other for the case $\beta < 1$. For $\beta > 1$, the locus crosses the negative real axis at the first resonance. Thus, the system is conditionally stable and the maximum gain is limited. For $\beta < 1$, the Nyquist plot is primarily located at the right hand side of the imaginary axis but, looking more closely, at higher frequencies the negative real axis is crossed and a large but again finite feedback gain could be used before the system becomes unstable. However, an ideal sensor-actuator is assumed here and, therefore, further limitations to the maximum feedback gain can be expected in practice, due to the real dynamics of the sensor and the actuator.

4.2. Performance

In this preliminary analysis, the performance of the control system is analysed in terms of: a) the VPSD at the centre of the radiating plate p_r; b) the pressure PSD at the centre of the cavity c_2.

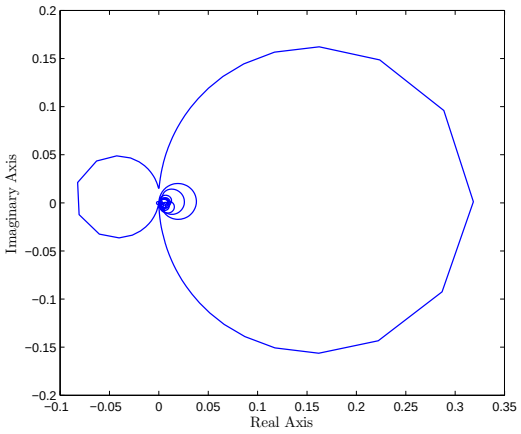

Figure 10. Nyquist Plot of the open loop sensor-actuator FRF for $\beta > 1$.

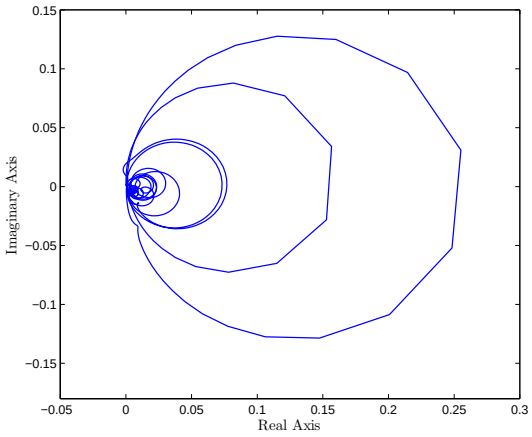

Figure 11. Nyquist Plot of the open loop sensor-actuator FRF for $\beta < 1$.

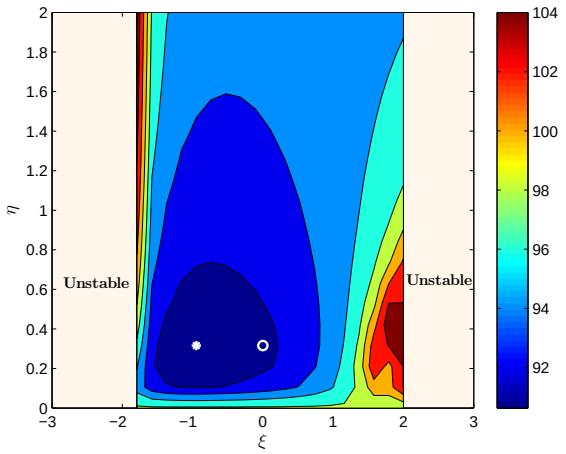

Figure 12. Frequency-averaged pressure PSD at the centre of c_2, for a TBL excitation, plotted versus ξ and η, for $\beta > 1$.

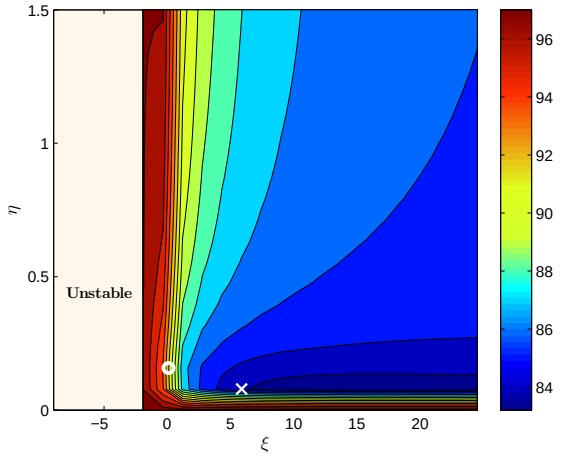

Figure 13. Frequency-averaged pressure PSD at the centre of c_2, for a TBL excitation, plotted versus ξ and η, for $\beta < 1$.

The corresponding results are shown in Fig. 14 and 16. Also, some frequency-averaged control performance metrics are used. To this end, the pressure (or the velocity) PSD at the centre of the cavity (or the panel) is integrated numerically over all frequencies. It can be seen in Fig. 12 - 13 that the broadband noise reduction performance is qualitatively similar to that observed with the reduced order model. In Fig. 12, as ξ moves closer to the stability limits the pressure increases; whereas, for $\beta < 1$, Fig. 13, the sound pressure in c_2 monotonically decreases with increasing the gain g (or ξ). The pressure PSD at the centre of c_2 is plotted versus frequency in Fig. 14 for three cases: without control, with passive control using c_p only, and finally with active control using both c_p and g. For the passive control, the optimally tuned damping coefficients given by the circles in Fig. 12 - 13 are used. For the active control case for $\beta > 1$ (red curves), the combination of active and passive damping ratios used is indicated by the white $*$. For the active control case for $\beta < 1$, the combination is designated by the white $\times$. Once again, the case $\beta < 1$ gives better isolation effects. In Fig. 15 - 16, the frequency-averaged VPSD versus ξ and η and the corresponding VPSD at the centre of p_r are shown in the case $\beta < 1$. Here, the

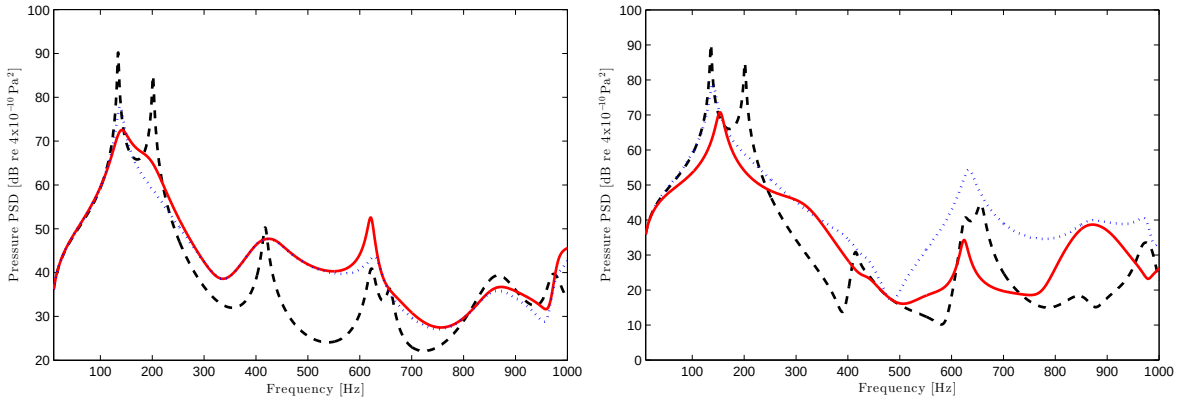

Figure 14. Pressure PSD at the centre of c_2. No control (- - - -), passive control (·····) and optimal tuned active control (——). Left hand side is for $\beta > 1$ and right hand side is for $\beta < 1$.

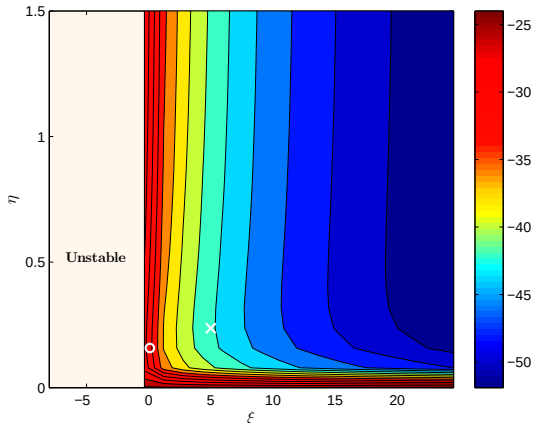

Figure 15. Frequency-averaged VPSD at the centre of p_r, for a stationary TBL excitation, plotted versus ξ and η. Case $\beta < 1$.

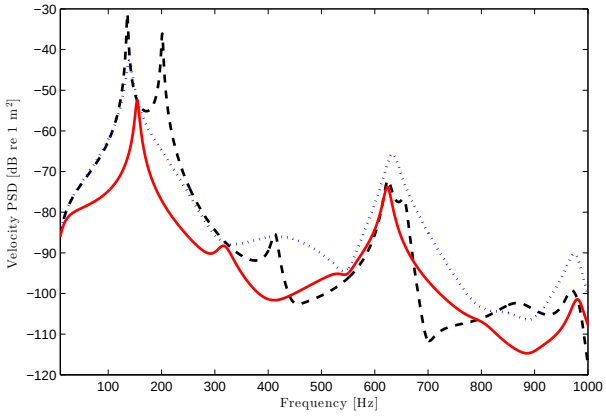

Figure 16. VPSD at the centre of p_r, for $\beta < 1$. No control (- - - -), passive control (·····) and optimal tuned active control (——).

damping coefficients used are given by the white $\times$ and the white $\circ$, shown in Fig. 15, for the active control and for the passive one, respectively.

In general, there is a slight increase in the high frequency amplitude response when the control is set on, as shown in Fig.14 and 16. This increase is particularly marked in the case $\beta > 1$. Nevertheless, large reductions of the interior sound levels can be expected at the lowest resonance frequencies. By comparing Fig. 16 to the right-hand side plot of Fig. 14, it can be concluded that the large contributions to the interior sound pressure are the two lowest double panel modes. This is why controlling vibrations of the radiating panel gives significant reductions of the sound pressure in the cavity c_2. The two modes are clearly the strongest contributors to the interior pressure. Thus significant frequency-averaged reductions are seen in plots Fig. 14 and 16 despite the small control spillover at higher frequencies.

5. Conclusions

The active control of TBL noise transmission through a coupled double panel system into an acoustic enclosure is investigated. The theoretical analysis of the control system stability is carried out. Closed form expressions for the stability limits are given for a reduced order model in terms of the minimal/maximal active damping ratio. For the increased order model, similar limits are found which only slightly change with the passive damping ratio. Afterwards, the performance of the active control system is analysed theoretically. The results are presented first for a point force excitation with white noise spectral distribution as a reference case and then for the stochastic TBL pressure distribution - both for the reduced and the increased order model. The behaviour of the control system is found to strongly depend on the ratio between the fundamental resonance frequencies of the two panels. The case when the fundamental resonance frequency of the source panel is larger than the fundamental resonance frequency of the radiating panel results in very promising sound transmission control effects. In particular, for a stationary TBL excitation, significant reductions of the low frequency vibrations of the radiating panel are predicted. Consequently, large sound pressure reductions in a broad frequency band in the acoustic cavity used to model the vehicle interior are predicted.

Acknowledgments

The research work of Anna Caiazzo has been funded by the European Commission within the ITN Marie Curie Action project BATWOMAN under the 7th Framework Programme (EC grant agreement no. 605867). The Research Fund KU Leuven is gratefully acknowledged for its support, as well as the IWT Flanders through the TUMULT project. The project has also received funding from the European Union's Horizon 2020 research and innovation programme under the Marie Sklodowska-Curie grant agreement no. 657539.

References

[1] Mixson J S and et al 1991 *Aeroacoustics of Flight Vehicles: Theory and Practice. Volume 2: Noise control*, ed H.H Hubbard, NASA Langley Research Center and et al, chapter 16 pp 271–335
[2] Wilby J F 1996 Aircraft interior noise *JSV* **190** 545–64
[3] Alujević N and et al 2011 Smart double panel for the sound radiation control: blended velocity feedback *AIAA Journal* **49** 1123–34
[4] Rohlfing J and Gardonio P 2014 Ventilation duct with concurrent acoustic feed-forward and decentralised structural feedback active control *JSV* **333** 630–45
[5] Misol M, Haase T and Monner H P 2014 *J. Acoust. Soc. Am.* **136** 1610–18
[6] Gardonio P and Alujević N 2010 Double panel with skyhook active damping control units for control of sound radiation *J. Acoust. Soc. Am.* **128** 1108–17
[7] Gardonio P and Zilletti M 2015 Sweeping tuneable vibration absorbers for low-mid frequencies vibration control *JSV* **354** 1–12
[8] Preumont A and et al 2002 Force feedback versus acceleration feedback in active vibration isolation *JSV* **257** 605–13
[9] Alujević N, Wolf H, Gardonio P and Tomac I 2011 Stability and performance limits for active vibration isolation using blended velocity feedback *JSV* **330** 4981–97
[10] Alujević N and et al 2015 Self-tuneable velocity feedback for active isolation of random vibrations in subcritical two degree of freedom systems *Acta Acust united Ac* **101** 950–63
[11] Bull M K 1996 Wall-pressure fluctuations beneath turbulent boundary layers: some reflections on forty years of research *JSV* **190** 299–315
[12] Corcos G M 1964 The structure of the turbulent pressure field in boundary-layer flows *J. Fluid Mech.* **18** 353–75
[13] Blake W K 1986 *Mechanics of flow-induced sound and vibration. Volume II.* (Orlando: Academic Press)
[14] Munich F P, Wien F G R and Palaiseau J S 2013 *Noise Sources in Turbulent Shear Flows: Fundamentals and Applications* (Udine: Springer)
[15] Da Rocha J, Suleman A and Lau F 2012 Prediction of turbulent boundary layer induced noise in the cabin of a BWB aircraft *Shock Vib.* **19** 693–705
[16] Goody M 2004 Empirical spectral model of surface pressure fluctuations *AIAA Journal* **42** 1788–1794

[17] Hwang Y F, Bonness W K and Hambric S A 2009 Comparison of semi-empirical models for turbulent boundary layer wall pressure spectra *JSV* **319** 199–217
[18] Da Rocha J and et al 2009 Prediction of flow-induced noise in transport vehicles: development and validation of a coupled structural-acoustic analytical framework *Can. Acoust.* **37** 13–29
[19] Graham W R *Proc. Conf. on Aeroacoustics: Boundary layer induced noise in aircraft* 1992 (Aachen) vol 1, pp 87–96.